Multiaxial fatigue experiments for elastomers based on true strain invariants

Etienne Le Mire, Erwan Verron, Bertrand Huneau, Nathan Selles

Journal of Rubber Research manuscript No.
(will be inserted by the editor)

Multiaxial fatigue experiments for elastomers based on true strain invariants

Etienne Le Mire · Erwan Verron · Bertrand Huneau · Nathan Selles

Received: date / Accepted: date

Abstract For decades, multiaxial fatigue tests have been proposed in order to derive models for fatigue life prediction of elastomers. Nevertheless, the importance of quantifying the multiaxiality has not sufficiently been discussed. In this paper, a new method is proposed to handle the multiaxiality in elastomers fatigue testing. It is based on the pair (K_2, K_3), two invariants of the Hencky (true) strain tensor. Thanks to the example of the simultaneous uniaxial tension-torsion fatigue of a Styrene Butadiene Rubber, we demonstrate that it is possible to prescribe a constant multiaxiality level throughout different tests. The method consists in fixing the multiaxiality indicator K_3, and then in varying the strain level with the intensity of distorsion indicator K_2. Results show that the fatigue lives seem to unify with K_2 regardless of the values of K_3. They also demonstrate that the initiation crack angle depends on the multiaxiality indicator K_3 but not on K_2. Finally, the relevance of the approach is acknowledged by comparing the pair (K_2, K_3) to the classical largest principal stretch ratio and biaxiality factor.

Keywords elastomers · fatigue · multiaxiality · uniaxial tension-torsion · Hencky strain invariants

1 Introduction

Rubber is used in a wide range of applications, including engine dampers, tires, joints in nuclear facilities, etc. In service, the majority of rubber components undergo cyclic mechanical loadings, inducing the progressive degradation of the material until failure: this phenomenon is called fatigue. When dealing with mechanical fatigue, rubber parts are subjected to very complex loading conditions whose characteristics (amplitude, frequency ...) can vary dramatically all along the life of the structure, rendering the life prediction very difficult. For about two decades, authors have proposed predictions of the fatigue life of rubber components, based on stress, strain, energy and/or other mechanical quantities. Even though of high interest, the prediction of fatigue life is not directly the issue of the current paper, and the reader can refer for example to Mars and Fatemi (2002), and Tee et al. (2018) for reviews, and André et al. (1999), Saintier et al. (2006), Ayoub et al. (2014), and Behroozinia et al. (2019) for recent advances.

Once models for fatigue life prediction are derived, a large quantity of fatigue tests results are necessary to identify their parameters. Practically, loading conditions are commonly divided into two categories: uniaxial loading conditions that apply along one given direction, and multiaxial loading conditions that apply along different directions. Even though structures in service rarely experience uniaxial loading conditions, several models have been proposed to predict the fatigue life of rubber-like materials under uniaxial loading conditions (Poisson et al., 2011; Wang et al., 2014; Juhre and Krause, 2015; Belkhiria et al., 2020). Nevertheless, due to the nature of the phenomenon of fatigue, it is not possible to capture its complexity under multiaxial loadings by only considering uniaxial experimental results; hence multiaxial fatigue tests are necessary. Simultaneous uniaxial tension-torsion experiments are the most widely used for multiaxial fatigue of elastomers. Several specimens have been specifically designed for these experiments: O-ring by Mars (2001a), diabolo-like samples with different curvature radii (Ostoja-Kuczynski et al., 2003; Le Cam et al., 2008; Ayoub et al., 2010), hollow diabolo-like

E. Le Mire
1 rue de la Noë 44300 Nantes
E-mail: Etienne.Le-Mire@ec-nantes.fr

E. Verron
1 rue de la Noë 44300 Nantes
E-mail: Erwan.Verron@ec-nantes.fr

B. Huneau
1 rue de la Noë 44300 Nantes
E-mail: Bertrand.Huneau@ec-nantes.fr

N. Selles
60 rue Auber 94408 Vitry-sur-Seine
E-mail: selles@lrccp.com

specimens (Wang et al., 2020), etc. Each of these samples has been designed to achieve specific properties such as the absence of buckling for compressive loadings or high triaxiality in the mid-plane, for instance.

But in the same way that, for example, a uniaxial tension test and a pure shear test with the same stretch ratio in the loading direction are not mechanically equivalent, the issue of the mechanical equivalence of two multiaxial fatigue tests has to be addressed. It can be simply summarized by the following question: "how to quantify the multiaxiality of fatigue tests in order to compare their results in a consistent manner?" Actually, one indicator has been used in some studies for the past two decades: the biaxiality ratio, denoted B by Mars (2001a), or n by Zine et al. (2006). For plane stress tests, it is defined as the ratio between the two largest principal true strains: $B = n = \ln(\lambda_2)/\ln(\lambda_1)$, with $\lambda_1 \geq \lambda_2$. Its main purpose is to classify fatigue tests in simple categories regarding its value: $B = -0.5$ for uniaxial tension, $B = 0$ for pure shear, and $B = 1$ for equibiaxial tension. However, when dealing with multiaxial tests, say uniaxial tension-torsion, B can take any value between -0.5 and 0, rendering the comparison between different tests difficult: can a multiaxial test characterized by $B = -0.4$ be compared to a multiaxial test characterized by $B = 0.25$? More generally, is B the optimal indicator of the multiaxiality?

In the present paper, we consider a new multiaxiality indicator referred to as K_3, which is one of the invariants of the Hencky (true) strain tensor proposed by Criscione et al. (2000). Coupled with a measure of the distortion (another invariant denoted K_2), we demonstrate that pairs (K_2, K_3) greatly help to design fatigue tests, and more specifically to ensure that different strain levels can be achieved while maintaining constant the multiaxiality throughout the tests. The paper is organized as follows: Section 2 introduces the kinematic equations of the uniaxial tension-torsion of a cylinder, and the parameters K_2 and K_3. In Section 3, the theoretical developments are applied to the fatigue of a synthetic rubber (Styrene Butadiene Rubber, SBR). Section 4 closes the paper with a discussion on the relevance of the new indicators.

2 Methods

In this section, we derive the kinematic equations of the simultaneous uniaxial tension-torsion of a perfect cylinder, and introduce the parameters $\{K_i\}_{i=1,2,3}$, which are the indicators proposed for a new description of intensity and multiaxiality in the design of fatigue tests.

2.1 Kinematics of the uniaxial tension-torsion of a perfect cylinder

The equations of the uniaxial tension-torsion of a perfect cylinder are derived in the following; they can be found in several previous studies, e.g. Rivlin (1949); Ogden (1984); Ciarletta and Destrade (2014); Murphy (2015).

The problem notations are summarized in Figure 1. It consists in the study of a perfect cylinder, whose dimensions are its length L and radius A in the undeformed state, which become l and a in the deformed state, respectively. A vertical displacement U and a twist angle α are both applied on the top surface, while the cylinder is fixed at the bottom surface. The material is supposed to be homogeneous, isotropic, and incompressible. The undeformed (or reference) configuration is denoted $(\mathcal{C}_0)$, and the actual deformed one is denoted $(\mathcal{C})$. The mapping χ transforms any point P_0 of $(\mathcal{C}_0)$ into P in $(\mathcal{C})$. In what follows, capital letters (R, Z, etc.) are used for quantities related to $(\mathcal{C}_0)$, and lowercase letters for quantities relative to $(\mathcal{C})$, unless otherwise mentioned. $(\boldsymbol{e_1}, \boldsymbol{e_2}, \boldsymbol{e_3})$ is the cartesian coordinate system, and two cylindrical coordinate systems are used: $(\boldsymbol{e_R}, \boldsymbol{e_\Theta}, \boldsymbol{e_Z})$ in the reference configuration and $(\boldsymbol{e_r}, \boldsymbol{e_\theta}, \boldsymbol{e_z})$ in the deformed one.

The mapping between reference and deformed configurations is defined by

$$r = R\lambda^{-0.5} \quad , \quad \theta = \Theta + \tau\lambda Z \quad , \quad z = \lambda Z, \tag{1}$$

where λ and τ are the stretch in the uniaxial tension direction and the twist angle per unit of deformed length, respectively:

$$\lambda = \frac{l}{L} \quad \text{and} \quad \tau = \frac{\alpha}{l} = \frac{\alpha}{\lambda L}. \tag{2}$$

The deformation gradient tensor is

$$\boldsymbol{F} = \frac{1}{\sqrt{\lambda}}(\boldsymbol{e_r} \otimes \boldsymbol{e_R} + \boldsymbol{e_\theta} \otimes \boldsymbol{e_\Theta}) + R\sqrt{\lambda}\tau \boldsymbol{e_\theta} \otimes \boldsymbol{e_Z} + \lambda \boldsymbol{e_z} \otimes \boldsymbol{e_Z}, \tag{3}$$

and the corresponding left Cauchy-Green strain tensor, $\boldsymbol{b} = \boldsymbol{F}\boldsymbol{F}^T$, is

$$\boldsymbol{b} = \frac{1}{\lambda}\boldsymbol{e_r} \otimes \boldsymbol{e_r} + \left(\frac{1}{\lambda} + \lambda^2\tau^2 r^2\right)\boldsymbol{e_\theta} \otimes \boldsymbol{e_\theta} + \lambda^2\tau r(\boldsymbol{e_\theta} \otimes \boldsymbol{e_z} + \boldsymbol{e_z} \otimes \boldsymbol{e_\theta}) + \lambda^2 \boldsymbol{e_z} \otimes \boldsymbol{e_z}. \tag{4}$$

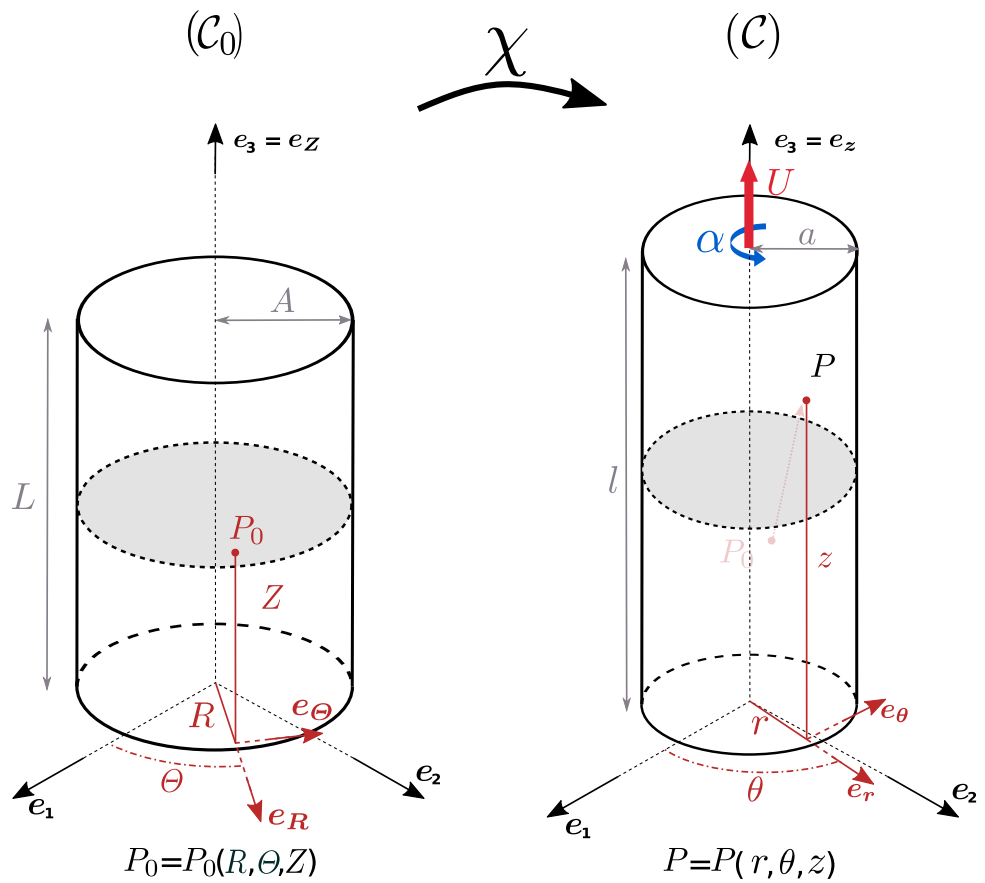

Fig. 1 Notations of the uniaxial tension-torsion of a perfect cylinder.

The principal stretch ratios $\{\lambda_i\}_{i=1,2,3}$ are the square roots of the eigenvalues of $\boldsymbol{b}$:

$$\begin{cases} \lambda_1 = \left[\frac{1}{2}\left(R^2\tau^2\lambda+\lambda^2+\frac{1}{\lambda} \right.\right. \\ \qquad \left.\left. -\sqrt{\left(R^2\tau^2\lambda+\lambda^2+\frac{1}{\lambda}\right)^2-4\lambda}\right)\right]^{0.5} \\ \lambda_2 = \lambda^{-0.5} \\ \lambda_3 = \left[\frac{1}{2}\left(R^2\tau^2\lambda+\lambda^2+\frac{1}{\lambda} \right.\right. \\ \qquad \left.\left. +\sqrt{\left(R^2\tau^2\lambda+\lambda^2+\frac{1}{\lambda}\right)^2-4\lambda}\right)\right]^{0.5} \end{cases} \tag{5}$$

2.2 Invariants of the Hencky strain tensor

The Hencky strain tensor, noted $\boldsymbol{H}$, is generally defined from the left stretch tensor, $\boldsymbol{V} = \sqrt{\boldsymbol{b}}$:

$$\boldsymbol{H} = \ln(\boldsymbol{V}) = \frac{1}{2}\ln(\boldsymbol{b}). \tag{6}$$

It is generally referred to as the true strain tensor.

The following derivation is based on the work of Criscione et al. (2000), in which the properties of $\boldsymbol{H}$ have been thoroughly investigated. One of the major advantages of $\boldsymbol{H}$ lies in its invariants, classically denoted $\{K_i\}_{i=1,2,3}$ and defined as

$$\begin{cases} K_1 = \ln(J) = \sum_{i=1}^{3}\ln(\lambda_i) \\ K_2 = \sqrt{\mathrm{dev}(\boldsymbol{H}):\mathrm{dev}(\boldsymbol{H})} = \sqrt{\sum_{i=1}^{3}\left(\ln(\lambda_i)-\frac{K_1}{3}\right)^2} \\ K_3 = \frac{3\sqrt{6}}{K_2^3}\prod_{i=1}^{3}\left(\ln(\lambda_i)-\frac{K_1}{3}\right) \end{cases} \tag{7}$$

where J is the Jacobian of the mapping χ, and $\mathrm{dev}(*) = (*) - \frac{1}{3}\mathrm{tr}(*)\boldsymbol{I}$ is the deviatoric operator. The physical meaning of $\{K_i\}_{i=1,2,3}$ is proposed by Criscione et al. (2000):

- K_1 defines the amount of volumetric dilatation.
- K_2 quantifies the intensity of the distortion the matter undergoes. It does not contain any measure of the dilatation, and is zero only if there is no distortion at the considered material point.
- K_3 indicates the mode of distortion. Note that K_3 is not defined for $K_2 = 0$, which is not prohibitive since in this case, matter does not undergo distortion, hence there is no mode of distortion. Table 1 presents the values of K_3 for simple deformation modes.

K_3	Deformation mode
-1	Uniaxial compression or equibiaxial tension
0	Planar tension (= pure shear)
1	Uniaxial tension or equibiaxial compression

Table 1 K_3 for simple deformation modes.

In the special case of incompressibility, $K_1 = 0$, and Eq. (7) simplifies into

$$\begin{cases} K_1 = 0 \\ K_2 = \sqrt{(\ln(\lambda_1))^2 + (\ln(\lambda_2))^2 + (\ln(\lambda_3))^2} \\ K_3 = \frac{3\sqrt{6}}{K_2^3} \ln(\lambda_1)\ln(\lambda_2)\ln(\lambda_3) \end{cases} \tag{8}$$

Substituting Eq. (5) into Eq. (8) gives a direct way to compute the values of K_2 and K_3 for any uniaxial tension-torsion loading conditions (λ, τ) applied to the cylinder. In appendix A, we provide a UVARM subroutine to be used within Abaqus to compute the values of K_1, K_2 and K_3 in finite element simulations.

Finally, Figure 2 presents the iso-contours of the multiaxiality indicator K_3 (dashed lines) and the iso-contours of the intensity indicator K_2 (solid lines). This graph is considered in the following to design fatigue tests.

3 Application to uniaxial tension-torsion fatigue tests of SBR

As an illustration of the new use of the parameters (K_2, K_3), we apply them to the fatigue response of a synthetic rubber. The present section describes and briefly discusses the results of the corresponding tests.

3.1 Material and sample

The material used in this study is a Styrene Butadiene Rubber (SBR), filled with 50 phr of N550 type carbon blacks, and vulcanized with sulfur. It is considered as an incompressible isotropic non-linear elastic material.

Fatigue tests were run on an Instron ElectroPuls E10000 machine which simultaneously applies a vertical displacement along the specimen revolution axis and a twist angle around the same axis, both being independently controlled. The specimen geometry is shown in Figure 3. It was designed by Lectez (2014) to achieve the two following objectives:

1. To concentrate strain in the cylindrical part of the sample in order to ensure that failure occurs in this zone.
2. On a given height around the mid-plane, the specimen behaves as a perfect cylinder subjected to uniaxial tension-torsion, as derived in Section 2.

3.2 Loading conditions

The relationships between the displacement U and the twist angle α prescribed to the specimen, and the corresponding stretch λ and angle per unit length τ that applies to the perfect cylinder are

$$\begin{cases} \lambda = 1 + \frac{U}{H_D}, & \text{(no unit)} \\ \tau = \frac{\alpha}{\lambda H_\alpha}, & \text{(rad.mm}^{-1}\text{)} \end{cases} \tag{9}$$

where $H_D = 30.3$mm and $H_\alpha = 25.6$mm are two geometric parameters which have been calculated by Lectez (2014).

As shown in Figure 4, all the input signals are in-phase sine, defined by their respective peek-to-peek values over a duty cycle: $U_{\max}$ for the displacement and $\alpha_{\max}$ for the twist angle. The cycles are fully relaxing, i.e. the minimum value of both displacement and twist is zero.

The end of life criterion is defined as a 50% drop in the maximum axial force measured over each cycle. The upper limit chosen for the number of cycles is 1 million cycles, in order to restrict the total duration of the experimental program. Finally, the frequency has been chosen as a compromise between self-heating and test duration: surface temperature was measured for all tests after 500 cycles, and no elevation of more than 15°C over the room temperature (23°C) was reported.

Table 2 summarizes the loading conditions of the fatigue tests. They can be divided into two groups:

K_3	$K_{2_{\max}}$	$U_{\max}$(mm)	$\alpha_{\max}(^\circ)$	Frequency (Hz)
0.5	0.45	3.51	167	1.75
	0.56	4.39	212	1
	0.66	5.23	257.5	0.75
1	0.5	12.92	0	1.25
	0.55	14.55	0	1
	0.64	17.79	0	0.75

Table 2 Loading conditions for fatigue tests.

uniaxial tension tests ($K_3 = 1$), and tests undergoing an intermediate state between uniaxial tension ($K_3 = 1$) and pure shear ($K_3 = 0$), i.e. with a targeted $K_3 = 0.5$. The values of K_2 have been chosen as close as possible for these two groups: they correspond to a compromise between the test duration distribution (ensuring results for short, medium, and long fatigue lives), self heating and machine availability. Practically, values of K_2 are computed analytically at the material point which undergoes the most damaging history, i.e. in the mid-plane at the external radius of the specimen ($Z = L/2, R = A$). Note that each test has been repeated 5 times.

The corresponding pairs (K_2, K_3) are reported in the iso-contours map of Fig. 2. All the uniaxial tension tests lie on the iso-line $K_3 = 1$, i.e. the horizontal axis, and all the multiaxial tests lie on the iso-line $K_3 = 0.5$. Moreover, experimental loading conditions lie on the corresponding iso-contours of K_2, rendering

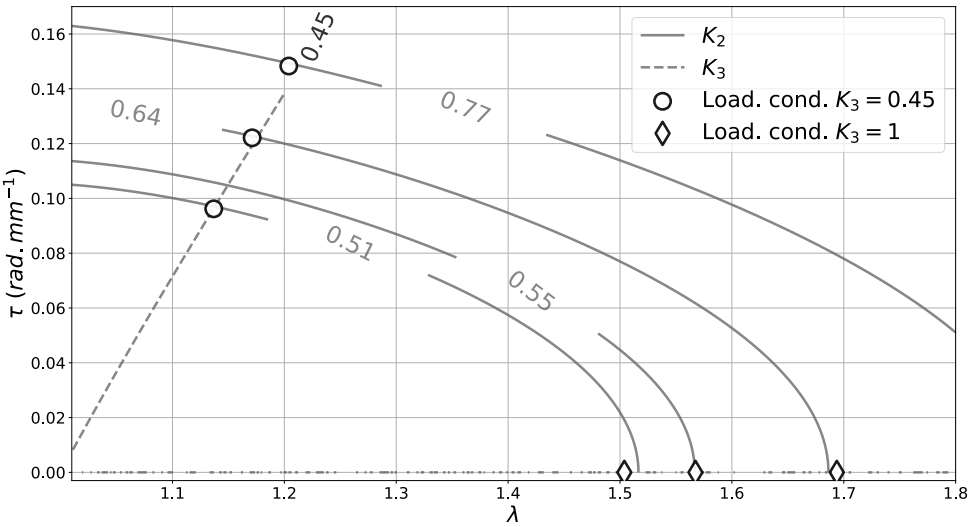

Fig. 2 Iso-K_2 and iso-K_3 in the space of the loading parameters (λ, τ). The loading conditions for $K_3 = 0.5$ and $K_3 = 1$ are also displayed.

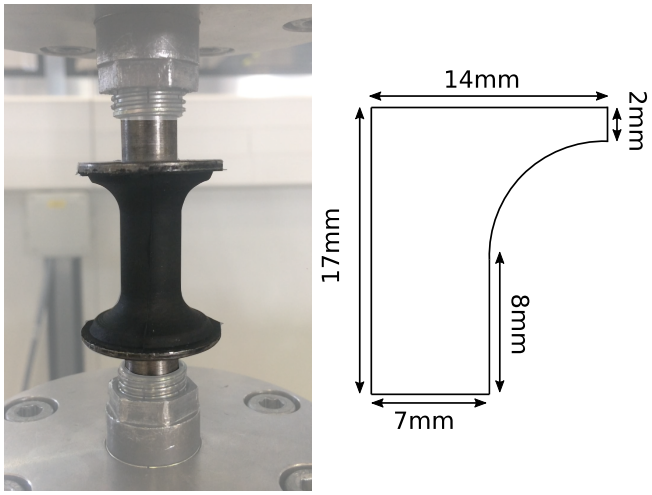

Fig. 3 Specimen mounted in the fatigue test machine E10 000 (left) and its dimensions without the metallic inserts (right).

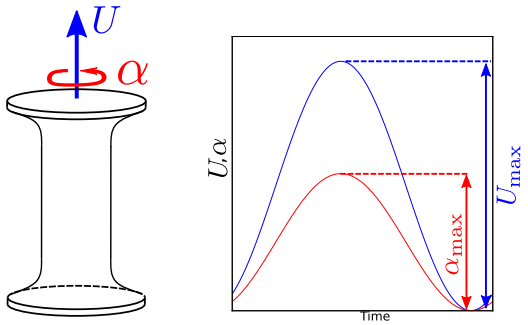

Fig. 4 Displacement U and twist angle α applied at the top surface of the specimen.

easy the reading of the plot: as loading conditions get farther from the origin, the intensity of the distortion increases.

3.3 Results

In the following, the results of the fatigue tests are presented. They consist in one Wöhler-like curve, where the numbers of cycle to failure are plotted against $K_{2_{\max}}$, and in crack angles at the locations where fatigue cracks are suspected to have initiated.

3.3.1 Fatigue life

Detailed fatigue tests results are available in Appendix B. They are plotted in Figure 5. The use of $K_{2_{\max}}$ as the fatigue life indicator seems natural, as it defines the amount of distortion prescribed to the specimen (see Section 3.2). Indeed, even if the trend for data corresponding to $K_3 = 1$ (for $K_2 = 0.55$ and 0.5) is not so clear, results of Figure 5 highlight that fatigue life increases as K_2 decreases. Moreover, K_2 seems to unify the results for both uniaxial tension and multiaxial fatigue tests, i.e. regardless of the value of K_3 is.

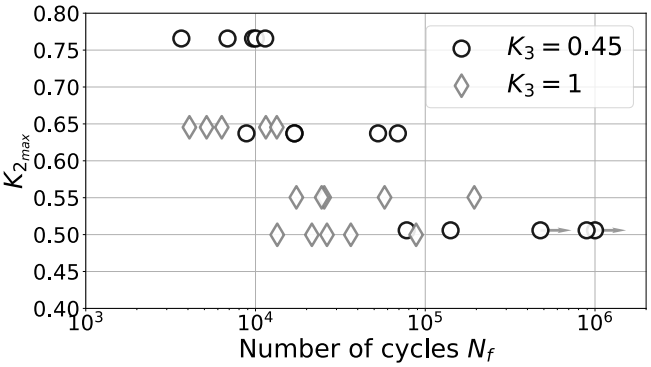

Fig. 5 $K_{2_{\max}} - N$ fatigue results for $K_3 \in \{0.5, 1\}$. Arrows represent censored data. One censored data point appears below 10^6 cycles, and is due to an overload of the computer's buffer during the test.

3.3.2 Crack initiation angle

As a final step, specimen surfaces have been analyzed with a numerical optical microscope Keyence VHX-6000 in order to determine the position of the suspected initiation sites, and to estimate the initiation

angle ω. Angles have been measured in the undeformed configuration, as explained in Figure 6.

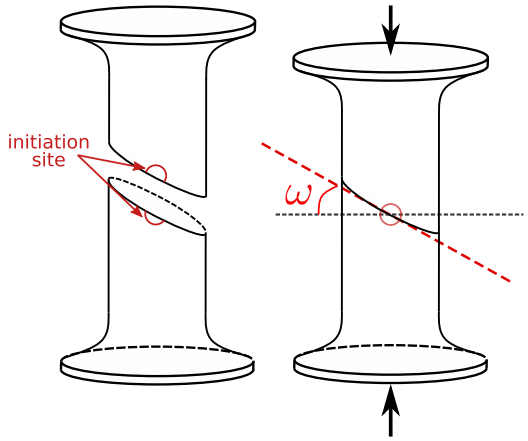

Fig. 6 Measurement of initiation angles after failure. The arrows represent a slight compression force that maintains the two broken parts together during measurement.

Except for three tests whose initiation occurred in the bulk, all tests led to initiation at the surface of the cylinder. Figure 7 presents the map of the initiation angles with respect to K_2. For uniaxial tension-torsion

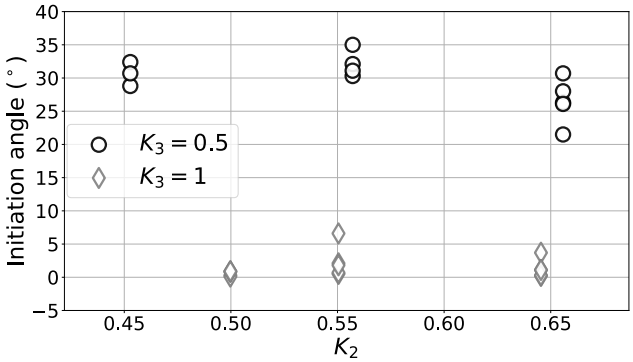

Fig. 7 Initiation angles vs. K_2 for both uniaxial tension and simultaneous uniaxial tension-torsion tests.

tests ($K_3 = 0.5$), all angles lie between 25° and 35° (except one just above 20°), whereas all uniaxial tension tests ($K_3 = 1$) have produced nearly horizontal angles (below 5°) except one.

All these observations were expected: during the uniaxial tension tests, the principal direction corresponding to both maximum stretch ratio and maximum stress coincides with the revolution axis of the specimen. Hence, cracks are expected to initiate in a plane perpendicular to this axis. Regarding the multiaxial tests, when the instant of maximum tension and twist is reached, the aforementioned principal directions are tilted, hence producing cracks that are oriented. Crack angles for pure torsion tests ($K_3 = 0$) have been studied by Saintier et al. (2006): they report that for prescribed torsion angles between 70° and 100°, all the measured crack initiation angles (using the same definition as in Figure 6) lie between 27° and 19°, respectively. Mars and Fatemi (2006) also point out that under very high shear strains (during a torsion test for instance), failure planes tend to be perpendicular to the specimen axis. Qualitatively, the present results are in good agreement with the aforementioned observations: superimposing uniaxial tension to torsion leads to higher crack angles. It must be noted that for both the uniaxial tension and multiaxial tests, the intensity of distortion K_2 has no influence on the crack angle. This further highlights the idea that K_3 is a relevant multiaxiality indicator: tests with different intensity of distortion (K_2) but same multiaxiality level (K_3) produce nearly identical crack angles.

4 Discussion

As mentioned in the introduction, another indicator (the biaxiality ratio B) has already been used in some studies, mainly in the ones dealing with the origin and subsequent developments of the Cracking Energy Density (CED) (Mars, 2001a,b; Zine et al., 2006). In these works, B is introduced for plane stress or plane strain problems as the ratio of the two largest principal true strain,

$$B = \frac{\ln(\lambda_2)}{\ln(\lambda_1)} \quad \text{or} \quad \lambda_2 = \lambda_1^B. \tag{10}$$

Considering incompressible materials, it leads to the following expression of the deformation gradient in the principal strain directions (here denoted $\{\boldsymbol{e_i}\}_{i=1,2,3}$):

$$\boldsymbol{F} = \lambda_1 \boldsymbol{e_1} \otimes \boldsymbol{e_1} + \lambda_1^B \boldsymbol{e_2} \otimes \boldsymbol{e_2} + \lambda_1^{-1-B} \boldsymbol{e_3} \otimes \boldsymbol{e_3}. \tag{11}$$

Figure 8 corresponds to Figure 2 on which iso-lines of λ_1 and B have been superimposed. For clarity's sake, values of K_3 and B do not correspond to the same mechanical states. λ_1 and K_2 iso-contours are similar: they both indicate the amount of distortion, but note that λ_1 only indicates the extension in the direction of the first principal direction, while K_2 encompasses all directions. B and K_3 iso-contours are similar as they both quantify the multiaxiality. Nevertheless, they differ by nature. Indeed, K_3 is an invariant of the true strain tensor and does not depend on the coordinate system. Computing B necessitates to calculate the principal stretch ratios but also to rank them. Practically, it has been used for incompressible material for which the knowledge of two first principal stretch ratios is sufficient (the third one being deduced from the incompressibility assumption, i.e. the product of the three principal stretch ratios is equal to one). Its use for compressible materials should be investigated.

5 Conclusion

The present paper has shown that the use of K_3 as a multiaxiality indicator of displacement controlled fatigue tests for elastomers is relevant, as compared to

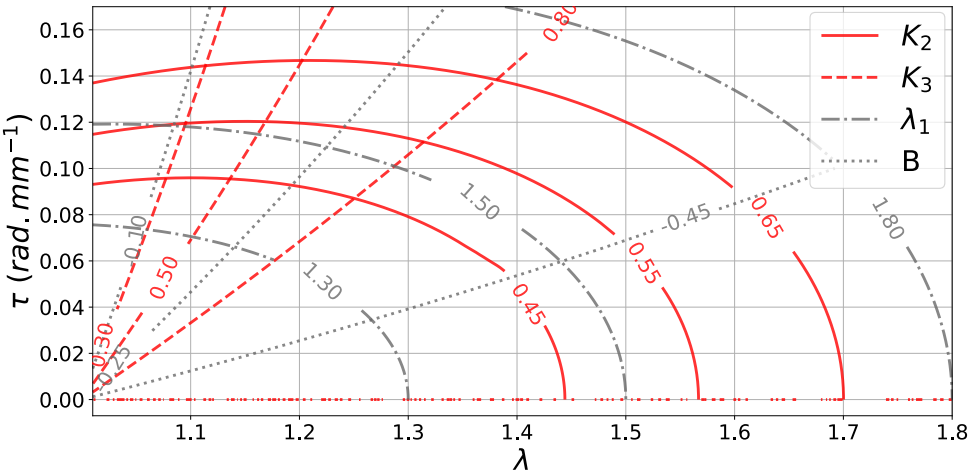

Fig. 8 Iso-K_2 and iso-K_3, along with iso-λ_1 and iso-B in the space of the loading parameters (λ, τ).

the classical biaxiality ratio B. Indeed, it derives from the invariants of the true strain tensor, hence it is insensitive to both the choice of the coordinate system and the ranking of the principal stretch ratios. The proposed method ensures that fatigue tests can be designed to maintain a consistent multiaxiality level, i.e. a constant value of K_3, which is an issue that has not been dealt with before. Introducing K_2 as the indicator of the intensity of the distortion, we argue that the pair (K_2, K_3) is a simple relevant tool to design fatigue experiments.

Conflict of interest

The authors declare that they have no conflict of interest.

References

André N, Cailletaud G, Piques R (1999) Haigh diagram for fatigue crack initiation prediction of natural rubber components. Kautsch Gummi Kunstst 52:120–123

Ayoub G, Naït-Abdelaziz M, Zaïri F, Gloaguen J (2010) Multiaxial fatigue life prediction of rubber-like materials using the continuum damage mechanics approach. Procedia Engineering 2(1):985–993, DOI 10.1016/j.proeng.2010.03.107

Ayoub G, Naït-Abdelaziz M, Zaïri F (2014) Multiaxial fatigue life predictors for rubbers: Application of recent developments to a carbon-filled SBR. International Journal of Fatigue 66:168–176, DOI 10.1016/j.ijfatigue.2014.03.026

Behroozinia P, Mirzaeifar R, Taheri S (2019) A review of fatigue and fracture mechanics with a focus on rubber-based materials. Proceedings of the Institution of Mechanical Engineers, Part L: Journal of Materials: Design and Applications 233(5):1005–1019, DOI 10.1177/1464420717719739

Belkhiria S, Hamdi A, Fathallah R (2020) Strain-based criterion for uniaxial fatigue life prediction for an SBR rubber: Comparative study and development. Proceedings of the Institution of Mechanical Engineers, Part L: Journal of Materials: Design and Applications pp 897–909, DOI 10.1177/1464420720913595

Ciarletta P, Destrade M (2014) Torsion instability of soft solid cylinders. The IMA Journal of Applied Mathematics 79(5):804–819, DOI 10.1093/imamat/hxt052

Criscione J, Humphrey J, Douglas A, Hunter W (2000) An invariant basis for natural strain which yields orthogonal stress response terms in isotropic hyperelasticity. Journal of the Mechanics and Physics of Solids 48(12):2445–2465, DOI 10.1016/S0022-5096(00)00023-5

Juhre D, Krause M (2015) A study on the influence of mechanical preconditioning on the fatigue behavior of rubber materials. In: Constitutive Models for Rubber IX, CRC Press, pp 439–444

Le Cam JB, Huneau B, Verron E (2008) Description of fatigue damage in carbon black filled natural rubber. Fatigue & Fracture of Engineering Materials & Structures 31(12):1031–1038, DOI 10.1111/j.1460-2695.2008.01293.x

Lectez AS (2014) Comportement multiaxial de pièces élastomères pré-contraintes. PhD thesis, DOI 10.1051/lhb/2010051, 0750077

Mars W (2001a) Cracking energy density as a predictor of fatigue life under multiaxial conditions. Rubber Chemistry and Technology 75:419–424, DOI 10.5254/1.3547670

Mars W (2001b) Multiaxial fatigue of rubber. PhD thesis

Mars W, Fatemi A (2002) A literature survey on fatigue analysis approaches for rubber. International Journal of Fatigue 24(9):949–961, DOI 10.1016/S0142-1123(02)00008-7

Mars W, Fatemi A (2006) Nucleation and growth of small fatigue cracks in filled natural rubber under multiaxial loading. Journal of Materials Science 41(22):7324–7332, DOI 10.1007/s10853-006-0962-2

Murphy J (2015) The stability of thin, stretched and twisted elastic rods. International Journal of Non-Linear Mechanics 68:96–100, DOI 10.1016/j.ijnonlinmec.2014.05.018

Ogden R (1984) Non-linear elastic deformations. Courier Corporation

Ostoja-Kuczynski E, Charrier P, Verron E, Marckmann G, Gornet L, Chagnon G (2003) Crack initiation in filled natural rubber: experimental database and macroscopic observations. In: Constitutive Models for Rubber III, CRC Press, pp 41–47

Poisson JL, Lacroix F, Meo S, Berton G, Ranganathan N (2011) Biaxial fatigue behavior of a polychloroprene rubber. International Journal of Jatigue 33(8):1151–1157, DOI 10.1016/j.ijfatigue.2011.01.014

Rivlin R (1949) Large elastic deformations of isotropic materials vi. further results in the theory of torsion, shear and flexure. Philosophical Transactions of the Royal Society of London Series A 242(845):173–195

Saintier N, André N, Cailletaud G, Piques R (2006) Crack nucleation and propagation under multiaxial fatigue in natural rubber. Int J Fatigue 28:61–72

Tee Y, Loo M, Andriyana A (2018) Recent advances on fatigue of rubber after the literature survey by Mars and Fatemi in 2002 and 2004. International Journal of Fatigue 110:115–129, DOI 10.1016/j.ijfatigue.2018.01.007

Wang X, Shangguan W, Rakheja S, Li W, Yu B (2014) A method to develop a unified fatigue life prediction model for filled natural rubbers under uniaxial loads. Fatigue & Fracture of Engineering Materials & Structures 37(1):50–61, DOI 10.1111/ffe.12081

Wang Y, Liu J, Duan W, Pan Z, Qiao Y (2020) Fatigue of vulcanized natural rubber under proportional and non-proportional loading. Fatigue & Fracture of Engineering Materials & Structures pp 2232–2246, DOI 10.1111/ffe.13250

Zine A, Benseddiq N, Naït-Abdelaziz M, Hocine NA, Bouami D (2006) Prediction of rubber fatigue life under multiaxial loading. Fatigue & Fracture of Engineering Materials & Structures 29(3):267–278, DOI 10.1111/j.1460-2695.2005.00989.x

A UVARM subroutine for the computation of K_1, K_2 and K_3 in Abaqus.

```
!!! This subroutine is used to compute
!!! the Ki that are quantities deriving
!!! from the Hencky strain tensor
!!! invariants (see Criscione et al. (2000))
      SUBROUTINE UVARM(UVAR,DIRECT,T,TIME,
     1 DTIME,CMNAME,ORNAME, NUVARM,NOEL,
     2 NPT,LAYER,KSPT,KSTEP,KINC,NDI,NSHR,
     3 COORD,JMAC,JMATYP,MATLAYO,LACCFLA)
C
      INCLUDE 'ABA_PARAM.INC'
C
      CHARACTER*80 CMNAME,ORNAME
      CHARACTER*3 FLGRAY(15)
      DIMENSION UVAR(NUVARM),DIRECT(3,3)
      DIMENSION T(3,3),TIME(2)
      DIMENSION ARRAY(15),JARRAY(15)
      DIMENSION JMAC(*),JMATYP(*),COORD(*)
      DIMENSION HENCK(6), PE(3), ANPE(3,3)
      INTEGER LSTR, NSHR, NDIR
      REAL K1, K2, K3
C
!!! Assign 'LE' to HENCK
        CALL GETVRM('LE',ARRAY,JARRAY,FLGRAY,
     1 JRCD,JMAC,JMATYP,MATLAYO,LACCFLA)
C
!!! Hencky strain tensor
      HENCK(1) = ARRAY(1)
      HENCK(2) = ARRAY(2)
      HENCK(3) = ARRAY(3)
      HENCK(4) = ARRAY(4)
      HENCK(5) = ARRAY(5)
      HENCK(6) = ARRAY(6)
      HENCK(7) = ARRAY(4) !Symmetric tensor
      HENCK(8) = ARRAY(5)
      HENCK(9) = ARRAY(6)
C
!!! Parameters for the function SPRIND
      NDIR = 3
      NSHR = 3
      LSTR = 2 ! 2 for the eigenvalues of a
               ! strain tensor
!!! SPRIND is used to compute the eigenvalues
!!! of a tensor. The result is assigned to PE
      CALL SPRIND(HENCK,PE,ANPE,LSTR,NDIR,NSHR)
C
!!! Compute the Ki using the principal
!!! extensions PE
      K1 = PE(1) + PE(2) + PE(3)
      K2 = ((PE(1))**2 + (PE(2))**2 +
     1     (PE(3))**2)**0.5
      K3 = 3*(6**0.5)*PE(1)*PE(2)*
     1     PE(3)/(K2**3)
C
!!! RESULTS
!!! K1, K2, K3
      UVAR(1) = K1
      UVAR(2) = K2
      UVAR(3) = K3
C
      RETURN
      END
```

B Fatigue tests results

K_3	n°	K_2	U_{max} (mm)	α_{max} ($^\circ$)	Freq. (Hz)	N_f	Surf. T ($^\circ C$) @ 500 cycles
0.5	1	0.45	3.51	167	1.75	1000000	34
	2	0.45	3.51	167	1.75	140994	32
	3	0.45	3.51	167	1.75	892646	32
	4	0.45	3.51	167	1.25	477000	-
	5	0.45	3.51	167	1.25	77749	31
	6	0.56	4.39	212	1	16984	33
	7	0.56	4.39	212	1	8843	33
	8	0.56	4.39	212	1	52712	32
	9	0.56	4.39	212	1	68971	33
	10	0.56	4.39	212	1	16944	33
	11	0.66	5.23	257.5	1	3657	37
	12	0.66	5.23	257.5	0.75	9670	32
	13	0.66	5.23	257.5	0.75	10046	35
	14	0.66	5.23	257.5	0.75	11405	31
	15	0.66	5.23	257.5	0.75	6843	31
1	16	0.50	12.92	0	1.25	88340	34.5
	17	0.50	12.92	0	1.25	13431	34
	18	0.50	12.92	0	1.25	21482	35
	19	0.50	12.92	0	1.25	26363	34
	20	0.50	12.92	0	1.25	36438	34
	21	0.55	14.55	0	1	25400	34
	22	0.55	14.55	0	1	24535	34
	23	0.55	14.55	0	1	57604	35
	24	0.55	14.55	0	1	194490	32
	25	0.55	14.55	0	1	17408	32
	26	0.64	17.79	0	0.75	6326	34
	27	0.64	17.79	0	0.75	11507	36
	28	0.64	17.79	0	0.75	5151	33
	29	0.64	17.79	0	0.75	13352	34
	30	0.64	17.79	0	0.75	4080	34

Table 3 Results of the fatigue tests.